

# Parametric X-ray radiation in the Smith-Purcell geometry for non-destructive beam diagnostics

O. D. Skoromnik<sup>a</sup>, I. D. Feranchuk<sup>b,c,d,\*</sup>, D. V. Lu<sup>e</sup>

<sup>a</sup>Max Planck Institute for Nuclear Physics, Saupfercheckweg 1, 69117 Heidelberg, Germany

<sup>b</sup>Atomic Molecular and Optical Physics Research Group, Advanced Institute of Materials Science, Ton Duc Thang University, 19 Nguyen Huu Tho Str., Tan Phong Ward, District 7, Ho Chi Minh City, Vietnam

<sup>c</sup>Faculty of Applied Sciences, Ton Duc Thang University, 19 Nguyen Huu Tho Str., Tan Phong Ward, District 7, Ho Chi Minh City, Vietnam

<sup>d</sup>Belarusian State University, 4 Nezavisimosty Ave., 220030, Minsk, Belarus

<sup>e</sup>Faculty of Physics, The University of Danang - University of Science and Education. B3 Building, 459 Ton Duc Thang, Lien Chieu, Da Nang, Vietnam

## Abstract

We investigate parametric X-ray radiation (PXR) under condition of the extremely asymmetric diffraction, when the ultra-relativistic electron bunch is moving in *vacuum* parallel to the crystal-vacuum interface, close to the crystal surface. This type of geometry coincides with the well known mechanism of generation of radiation, when the self-field of the particle beam interacts with the reflecting metal grating, namely the Smith-Purcell effect. We demonstrate that in this geometry the main contribution is given via a tail region of the beam distribution, which penetrates the crystal and X-rays are radiated along the normal to the crystal surface. We determine the electron beam characteristics, when this phenomenon can be observed. It is essential that in this geometry the majority of electrons does not undergo multiple scattering and consequently the characteristics of the particle beam are not changed, thus allowing the usage of the emitted X-rays for the purpose of non-destructive beam diagnostics, which can complement the traditional knife-edge method.

**Keywords:** parametric X-ray radiation, Smith-Purcell effect, dynamical diffraction, extremely asymmetric diffraction  
**PACS:** 41.50+h, 41.60-m

## 1. Introduction

Parametric X-ray radiation (PXR) is generated when a charged particle moves uniformly in a periodic medium [1, 2]. The typical property of this type of radiation is that it is emitted under the large angle to the velocity of the charged particle. In addition, it is characterized by high brightness, narrow spectral interval and possibility to uniformly tune the frequency of the radiated photons. Moreover, the intensity of radiation is relatively weakly dependent on the particle energy. Furthermore, the large angle of the emitted photons allows one to employ non-conventional geometries, which can lead to the improvements of the various characteristics of the emitted radiation [3].

Recently, it was demonstrated [4] that the intensity of the radiation can be significantly increased if the grazing geometry under condition of the extremely asymmetric diffraction of the emitted photons (PXR-EAD) is employed. However, in that case the electrons were moving

inside a crystal, parallel to the crystal vacuum interface. Consequently, in that situation the effective length of the electron trajectory, which contributes to the formation of PXR is bounded from above by the multiple scattering on atoms of the medium, which the bunch of electrons exhibits moving inside the crystal.

For this reason, it is essential to investigate the geometry, in which the whole crystal length contributes to the intensity, but the limiting factor of multiple electron scattering is removed. The most natural way is to consider that the electron beam is moving *outside* of a crystal in vacuum, at a small distance to it, but still parallel to the crystal-vacuum interface. This geometry corresponds to the Smith-Purcell effect [5, 6], but in the X-ray frequency range due to the parametric radiation mechanism (PXR-SPG). In this case the electronic density of a crystal corresponds to the metal surface grating, interaction with which generates the radiation in optical or microwave ranges [7, 8] and for X-rays [9, 10]. For this reason, the radiation field is formed due to the diffraction of the electron beam self-field on the periodic electronic density of the crystal. Consequently, the determination of the characteristics of PXR-SPG, the discussion of its possible observation and applications for the beam diagnostics [11]

\*Corresponding author

Email addresses: ods@mpi-hd.mpg.de (O. D. Skoromnik),  
 ilya.feranchuk@tdtu.edu.vn (I. D. Feranchuk)

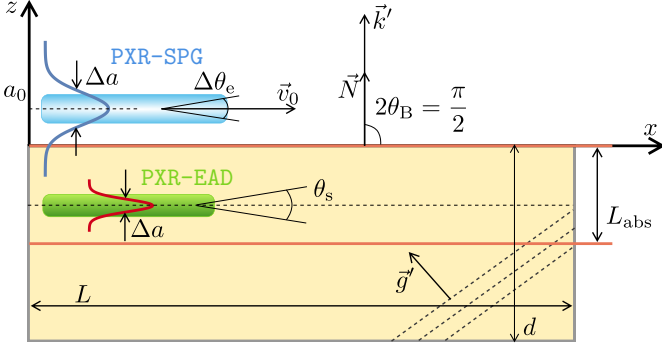


Figure 1: (Color online) The comparison of the grazing geometry of PXR-EAD, when an electron beam moves in a *crystal* with the grazing geometry of PXR-SPG, when the main beam part propagates in *vacuum* and only the halo of the beam travels inside a crystal. In both cases an electron beam propagates with the velocity  $\vec{v}_0$  along the  $\langle 110 \rangle$ . The emitted radiation exits from a crystal in the direction  $\vec{k}' = \omega \vec{v}_0 / v_0^2 + \vec{g}$  and is not absorbed. Here  $\theta_s$  is the mean square angle of multiple-electron scattering in a crystal.  $a_0$  is the beam impact parameter,  $\Delta a$  is the transverse spread of the beam due to its emittance and  $\vec{g}$  is the reciprocal lattice vector for planes where PXR is formed.

are the main goals of the present work.

## 2. Qualitative consideration

In order to discuss the qualitative peculiarities of the considered phenomenon let us assume that the monocrystal plate of a thickness  $d$  and a length  $L$  is used to produce PXR-SPG. We also suppose that the crystal length  $L \gg d$ , but the X-ray absorption length  $L_{\text{abs}} < d$ . In Fig. 1 we demonstrate the electron trajectories and compare the grazing geometry of PXR-EAD, i.e., when an electron moves *inside* the crystal parallel to the crystal-vacuum interface with the grazing geometry of PXR-SPG when an electron moves in *vacuum* and also parallel to the crystal-vacuum interface. In addition, we suppose that in the case of PXR-SPG the electrons move closely to the crystal surface, such that their own electromagnetic field penetrates the crystal. Following Refs. [2, 4] we now estimate the number of radiated photons in both cases. Let the quantity  $Q_{\text{PXR}}$  describes the number of photons emitted from the unit length of an electron trajectory for the transition geometry case. Then the total number of PXR photons is bounded by the X-ray absorption length  $L_{\text{abs}}$  [1] and equals to

$$N_{\text{PXR}} = Q_{\text{PXR}} L_{\text{abs}}. \quad (1)$$

The actual expression for  $Q_{\text{PXR}}$  is not important and for our qualitative estimation we mention only that  $Q_{\text{PXR}}$  is independent of the crystal length under the condition  $L_{\text{abs}} < d$  [2].

In the case of PXR-EAD [4] the photons emitted from the whole length  $L$  of an electron trajectory contribute to the formation of PXR, as they are not absorbed. Moreover, according to Ref. [4] the number of emitted photons

$N_{\text{PXR-EAD}}$  in this situation significantly exceeds  $N_{\text{PXR}}$ . One can obtain the following estimation in this case

$$N_{\text{PXR-EAD}} = Q_{\text{PXR-EAD}} L = 10^2 N_{\text{PXR}}. \quad (2)$$

For the estimation of the number of photons  $N_{\text{PXR-SPG}}$  of PXR-SPG we can use an analogous approach. First of all we notice that in the Smith-Purcell geometry, due to the beam emittance, a part of an electron beam (beam halo) is moving inside a crystal and generates radiation according to PXR-EAD. At the same time the major part of the beam is moving above the crystal surface and radiates according to the Smith-Purcell effect ( $N_{\text{SP}}$ ). As a result the total number of the emitted photons can be estimated in the following way

$$N_{\text{PXR-SPG}} = p_i N_{\text{PXR-EAD}} + p_o N_{\text{SP}}, \quad (3)$$

$$p_i + p_o = 1,$$

where  $p_i$  is the probability that the electron of a beam is moving inside the crystal and  $p_o$  is the corresponding probability when an electron moves in vacuum. We mention here that when the beam impact parameter  $a_0 \leq 0$ ,  $N_{\text{PXR-SPG}}$  coincides with  $N_{\text{PXR-EAD}}$ . Now let us estimate the quantity  $N_{\text{SP}}$  in the ideal case of vanishing emittance  $\epsilon = 0$ . In this situation, when crystal parameters are fixed  $N_{\text{SP}}$  strongly depends on the impact parameter  $a_0$ . Consequently,

$$N_{\text{SP}} = Q_{\text{SP}} L_{\text{SP}}(a_0), \quad (4)$$

where we introduced the coherent length  $L_{\text{SP}}$  for this process. This length is independent of the multiple electron scattering (electrons are moving in vacuum). For its determination one can use the following fact. It is well known [12] that the Fourier component of an electromagnetic self-field of an electron, corresponding to the wave length  $\lambda$ , in the direction perpendicular to the electron velocity is located inside the region of an angular spread  $\theta_{\text{tr}}$  and the characteristic size  $a_{\text{tr}}$ , for which one can write

$$\theta_{\text{tr}} \approx \gamma^{-1}, \quad a_{\text{tr}} \approx \frac{\lambda \gamma}{2\pi}, \quad \gamma = \frac{E}{mc^2}. \quad (5)$$

In the X-ray frequency range the characteristic size can reach the value  $a_{\text{tr}} = 10^{-5}$  cm, when the particle energy  $E \approx 10^3$  MeV.

For the following we assume that the bunch of electrons is moving in vacuum parallel to the crystal-vacuum interface under the distance  $a_0$ , which is smaller than  $a_{\text{tr}}$ , i.e.,  $a_0 < a_{\text{tr}}$ . If this condition is not fulfilled the intensity of the emitted radiation is exponentially suppressed, see below. This bunch of electrons has a transverse size  $\Delta a$ ,  $\Delta a < a_{\text{tr}}$  and the angular spread  $\Delta \theta_e$  that correspond to the natural emittance  $\epsilon = \Delta a \Delta \theta_e$ , see Fig. 1. Consequently, the coherent length  $L_{\text{SP}}$  can be defined as the length of an electron trajectory when the electron self-field still penetrates the crystal and therefore can diffract on the

electronic density of its atoms. In the ideal case of vanishing transverse spread  $\Delta a = 0$  this interaction takes place along the whole crystal length that is

$$L_{\text{SP}}(a_0) = L, \quad a_0 < a_{\text{tr}}, \quad \Delta a = 0. \quad (6)$$

However, in the realistic situation of a non-vanishing emittance the actual value of the coherent length is substantially restricted by the actual angular and transverse spreads of experimentally available electron bunches. As follows from Fig. 1 one can write the following estimation

$$L_{\text{SP}} = \frac{a_{\text{tr}}}{\Delta\theta_e} \leq \frac{a_{\text{tr}}^2}{\Delta a \Delta\theta_e} = \frac{\lambda^2 \gamma^2}{4\pi^2 \epsilon}, \quad a_0 < \frac{\lambda \gamma}{2\pi}. \quad (7)$$

For the numerical considerations we employ the characteristics of the Mainz microtron MAMI [13, 14]. As a result for the radiation wavelength  $\lambda = 3 \times 10^{-8}$  cm, the emittance  $\epsilon = 3 \times 10^{-7}$  cm and  $\gamma = 2 \times 10^3$  the coherent length reaches

$$L_{\text{SP}} \approx 10^{-3} \text{ cm}, \quad (8)$$

which is comparable with  $L_{\text{abs}}$ . These estimations are justified for the photons that are emitted in the cone with the angle  $\theta < \theta_{\text{tr}}$ .

Let us now estimate the number of photons  $Q_{\text{SP}}$  emitted from the unit length of a trajectory for the SP and compare its value with the  $Q_{\text{PXR}}$ . For this we notice [1, 15, 16] that the angular spread of the PXR is defined via a parameter

$$\theta_{\text{ph}} = \sqrt{\gamma^{-2} + \theta_s^2 + |\chi'_0|}, \quad (9)$$

where  $\theta_s$  is the mean square of the electron scattering angle and  $\chi'_0$  is the real part of the dielectric susceptibility of a crystal. Moreover, according to Ref. [1] the  $Q_{\text{PXR}}$  is defined as

$$Q_{\text{PXR}} \approx \left( \frac{\theta_{\text{D}}}{\theta_{\text{ph}}} \right)^4 A. \quad (10)$$

Here  $\theta_{\text{D}} \approx \theta_{\text{ph}}$  is the detector aperture and  $A$  is the quantity, which depends only on the parameters of the crystal.

Analogously, for SP the detector aperture angle  $\theta_{\text{D}}$  is limited by  $\theta_{\text{tr}}$  and for the angular width of the SP peak one can write

$$\theta_{\text{ph}}^{(0)} = \sqrt{\gamma^{-2} + |\chi'_0|}, \quad (11)$$

where we omitted the electron scattering angle, since in the SP case there is no multiple electron scattering as electrons are moving in vacuum. Consequently, we can write an analogous expression to Eq. (11), but for the SP

$$Q_{\text{SP}} = \left( \frac{\theta_{\text{tr}}}{\theta_{\text{ph}}^{(0)}} \right)^4 A = \left( \frac{1}{\gamma \theta_{\text{ph}}^{(0)}} \right)^4 A. \quad (12)$$

Consequently, the combination of Eqs. (3), (7) and (12) yields

$$N_{\text{SP}} = \frac{1}{\gamma^2 (\theta_{\text{ph}}^{(0)})^4} \frac{\lambda^2}{4\pi^2 \epsilon L_{\text{abs}}} N_{\text{PXR}}. \quad (13)$$

The estimation according to Eq. (13) for the MAMI microtron demonstrates that the total number of emitted photons of SP is significantly lower than the corresponding number for PXR and PXR-EAD:

$$N_{\text{SP}} \approx 10^{-2} N_{\text{PXR}} \approx 10^{-4} N_{\text{PXR-EAD}}. \quad (14)$$

Consequently, even if the small number of electrons from a tail region of the beam distribution appears inside the crystal, exactly these electrons will determine the total intensity of PXR-SPG ( $p_i \sim 10^{-2} p_o$ )

$$N_{\text{PXR-SPG}} \approx p_i N_{\text{PXR-EAD}}. \quad (15)$$

Formulas (11) and (13) allow one to determine the required normalized emittance for the number of emitted quanta  $N_{\text{SP}}$  to be comparable with  $p_i N_{\text{PXR-EAD}} = N_{\text{PXR}}$

$$\gamma \epsilon < \frac{1}{\gamma (|\chi'_0|)^2} \frac{\lambda^2}{4\pi^2 L_{\text{abs}}}. \quad (16)$$

For the radiation wavelength  $\lambda = 3 \times 10^{-8}$  cm,  $\gamma = 2 \times 10^3$  and Si crystal it leads to the condition

$$\gamma \epsilon \leq 10^{-8} \text{ cm} \times \text{rad}, \quad (17)$$

which is unreachable for modern accelerators.

The above qualitative analysis demonstrates that the intensity of PXR-SPG is mainly defined by the radiation of the electrons from the beam halo, which move inside a crystal. As a result one can exploit this feature for the non-destructive diagnostics of the electron beam.

In order to confirm these estimations we provide a rigorous calculation of the spectral angular distribution of  $N_{\text{PXR-SPG}}$  and the total number of emitted quanta based on the dynamical diffraction theory, which we discuss in the subsequent sections.

### 3. Spectral-angular distribution and integral intensity of PXR-SPG

In this section we will apply the dynamical theory of diffraction in order to calculate the intensity of PXR-SPG. However, we would like to notice that we use a special approach to the solution of a radiation problem, which was developed earlier in Refs. [1, 16–18]. In the majority of works, devoted to this problem when the interface between two media exists, the Maxwell equations are solved for each media independently. Then the resulting solution is represented as a linear combination of two linearly independent solutions  $\vec{E}_i^{(1)}$  and  $\vec{E}_i^{(2)}$  of the homogeneous equations and the solution  $\vec{E}_i^{(\text{in})}$  of the inhomogeneous ones. The solution

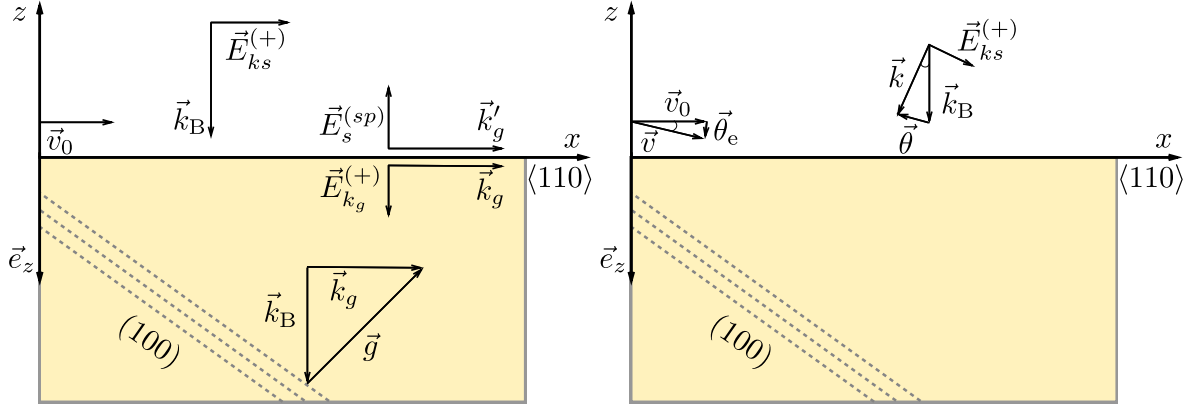


Figure 2: (Color online) Left pane: The grazing geometry of PXR-SPG in the ideal case, when the Wulff–Bragg’s condition for the emitted photons is fulfilled and propagation directions of incident, diffracted and diffracted-reflected waves. The angle  $\theta_0$  is the angle between  $\vec{v}_0$  and the  $x$ -axis and in the ideal case  $\theta_0 = 0$ . Right pane: Non ideal case. The deviation from the Wulff–Bragg’s condition and the variation of the velocity of the center of the beam are described by the vectors  $\vec{\theta}$  and  $\vec{\theta}_e$  respectively. In this pane the diffracted and diffracted-reflected waves are not shown. In both panes the incident wave  $\vec{E}_{k_s}^{(+)}$  describes the emitted PXR field in accordance with the reciprocity theorem Eq. (28).

$\vec{E}_i^{(\text{in})}$  is given via a current, formed by a charged particle in the corresponding medium. Here the index  $i$  numerates different media. Consequently, in this approach we can write down the general solution for the electromagnetic field in each medium as a linear combination

$$\vec{E}_i(\vec{r}, t) = C_i^{(1)} \vec{E}_i^{(1)}(\vec{r}, t) + C_i^{(2)} \vec{E}_i^{(2)}(\vec{r}, t) + \vec{E}_i^{(\text{in})}(\vec{r}, t). \quad (18)$$

The electromagnetic field  $\vec{E}_i(\vec{r}, t)$  is then plugged in into the boundary conditions of electrodynamics, which leads to the system of linear inhomogeneous equations for the coefficients  $C_i^{(1,2)}$ . The solutions of these equations are expressed through  $\vec{E}_i^{(\text{in})}(\vec{r}, t)$  and define the intensity of the radiation at a large distance from the crystal. However, the construction of a particular solution of inhomogeneous equations is rather a difficult step.

In our work we will employ a different approach [1, 16–18], which is based on the solution of the homogeneous equations and a Green function in an inhomogeneous medium in the whole space. Thus, for reader’s convenience we quickly revise below this procedure.

We are interested in the solution of the Maxwell’s equations

$$\text{rot rot } \vec{E}(\vec{r}, t) + \frac{1}{c^2} \frac{\partial^2 \vec{D}(\vec{r}, t)}{\partial t^2} = -\frac{4\pi}{c^2} \frac{\partial \vec{j}(\vec{r}, t)}{\partial t}, \quad (19)$$

or introducing the Fourier components

$$\text{rot rot } \vec{E}(\vec{r}, \omega) - \frac{\omega^2}{c^2} \vec{D}(\vec{r}, \omega) = i\omega \frac{4\pi}{c^2} \vec{j}(\vec{r}, \omega), \quad (20)$$

$$\vec{j}(\vec{r}, \omega) = \frac{e_0}{2\pi} \int dt \vec{v}_0(t) \delta[\vec{r} - \vec{r}_0(t)] e^{i\omega t}. \quad (21)$$

The tensor of dielectric permittivity  $\epsilon_{\alpha\beta}(\vec{r}, \vec{r}_1, \omega)$  of a medium relates the components of the induction vector

$D_\alpha(\vec{r}, \omega)$  with the components  $E_\alpha(\vec{r}, \omega)$  of the electromagnetic field strength:

$$D_\alpha(\vec{r}, \omega) = \int d\vec{r}_1 \epsilon_{\alpha\beta}(\vec{r}, \vec{r}_1, \omega) E_\beta(\vec{r}_1, \omega). \quad (22)$$

The dielectric permittivity tensor takes into account the boundaries between media. In our case of vacuum and a crystal this means that in vacuum  $\epsilon_{\alpha\beta}(\vec{r}, \vec{r}_1, \omega) = \delta_{\alpha\beta} \delta(\vec{r} - \vec{r}_1)$  and

$$\epsilon_{\alpha\beta}(t, \vec{r}, \vec{r}') = \sum_{\vec{g}} \int d\omega \int d\vec{k} \epsilon_{\alpha\beta}(\vec{k}, \vec{k} + \vec{g}, \omega) \times e^{i\vec{k} \cdot (\vec{r} - \vec{r}') - i\omega t - i\vec{g} \cdot \vec{r}}$$

in the crystal respectively. The Fourier components

$$\epsilon_{\alpha\beta}(\vec{k}, \vec{k} + \vec{g}, \omega)$$

in this expression correspond to the periodic distribution of the electronic density and are determined by the reciprocal lattice vectors  $\vec{g}$ .

We now define the Green function of the Maxwell’s equations

$$\epsilon_{\alpha\beta\gamma} \epsilon_{\gamma\mu\nu} \frac{\partial^2}{\partial x_\beta \partial x_\mu} G_{\nu\lambda}(\vec{r}, \vec{r}', \omega) - \frac{\omega^2}{c^2} \int d\vec{r}_1 \epsilon_{\alpha\beta}(\vec{r}_1, \vec{r}', \omega) G_{\beta\lambda}(\vec{r}, \vec{r}', \omega) = \delta_{\alpha\lambda} \delta(\vec{r} - \vec{r}') \quad (23)$$

where  $\epsilon_{\alpha\beta\gamma}$  is a Levi-Civita tensor. The Greek indices in Eq. (23) are running as  $1 \dots 3$  and a summation over repeated indices is understood. We consider only the spontaneous emission, which vanishes in the absence of the current. Consequently, with the help of the introduced Green function one can write down the expression for the electromagnetic field

$$E_\alpha(\vec{r}, \omega) = i\omega \frac{4\pi}{c^2} \int d\vec{r}' G_{\alpha\beta}(\vec{r}, \vec{r}', \omega) j_\beta(\vec{r}', \omega). \quad (24)$$

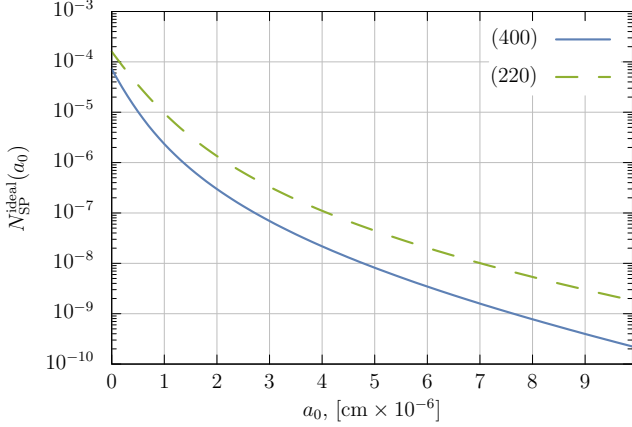


Figure 3: (Color online) The dependence of the Smith-Purcell photons  $N_{\text{SP}}^{\text{ideal}}$  on the distance  $a_0$  between the center of the electron beam and the crystal surface for the MAMI experimental facility in the ideal case of a vanishing emittance for the (220) and (400) reflections. The parameters of the reflections are given via Eqs. (61) and (62). The crystal length  $L = 1$  cm and the electron beam energy 900 MeV.

In order to determine the radiation field in the far zone, where a detector of X-ray photons is located we need to perform an asymptotic expansion in the limit  $r \gg r'$  in the Green function [1]. The resulting expression then reads

$$G_{\alpha\beta}(\vec{r}, \vec{r}', \omega) \approx \frac{e^{ikr}}{4\pi r} \sum_{s=1,2} e_{s\alpha} E_{ks\beta}^{(-)*}(\vec{r}', \omega), \quad (25)$$

$$\vec{k} = \frac{\omega}{c} \frac{\vec{r}}{r},$$

where  $\vec{e}_s$  are the polarization vectors and the fields  $E_{ks\beta}^{(-)*}(\vec{r}', \omega)$  satisfy the homogeneous Maxwell's equations

$$(\text{rot rot } \vec{E}_{ks}^{(-)*}(\vec{r}, \omega))_{\alpha} - \frac{\omega^2}{c^2} \int d\vec{r}_1 \epsilon_{\alpha\beta}^*(\vec{r}, \vec{r}_1, \omega) E_{ks\beta}^{(-)*}(\vec{r}_1, \omega) = 0. \quad (26)$$

It is important to stress here that the electromagnetic field  $\vec{E}_{ks}$  emitted by the particle inside a crystal possesses an asymptotic behavior for  $r \rightarrow \infty$  of a plane wave and an ingoing spherical wave

$$\vec{E}_{ks}^{(-)*}(\vec{r}, \omega) \approx \vec{e}_s e^{i\vec{k} \cdot \vec{r}} + \vec{f}_s \frac{e^{-ikr}}{r}, \quad r \rightarrow \infty. \quad (27)$$

Here  $\vec{f}_s$  are the scattering amplitudes, which are independent of  $r$ .

In contrast, when an external electromagnetic field is scattered or diffracted on a crystal, this wave possesses an asymptotic behavior of outgoing spherical wave, which is usually denoted as  $\vec{E}_{ks}^{(+)}(\vec{r}, \omega)$ . However, the wave  $\vec{E}_{ks}^{(-)*}(\vec{r}, \omega)$  and the wave  $\vec{E}_{ks}^{(+)}(\vec{r}, \omega)$  are related to each other with the following formula

$$(\vec{E}_{ks}^{(-)}(\vec{r}, \omega))^* = \vec{E}_{-\vec{k}s}^{(+)}, \quad (28)$$

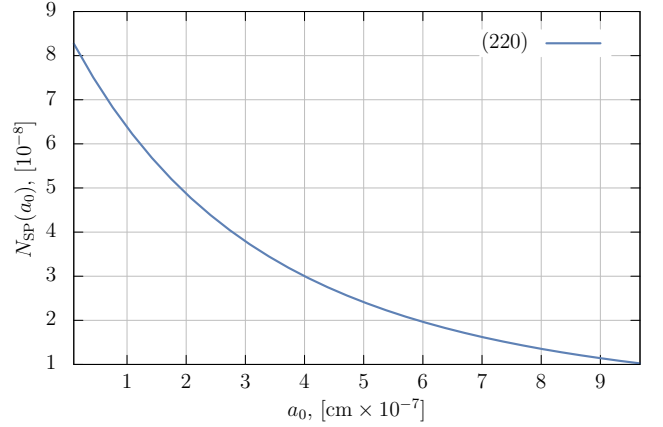


Figure 4: (Color online) The dependence of the Smith-Purcell photons  $N_{\text{SP}}$  on the distance  $a_0$  between the center of the electron beam and the crystal surface for the MAMI experimental facility and the (220) reflection. Here  $\Delta a = a_0/2$  and changes with  $a_0$ . The parameters of the reflection (220) are given via Eq. (62). The crystal length  $L = 1$  cm, the angle  $\theta_0 = 10^{-5}$  rad and the electron beam energy 900 MeV.

which is the analog of the well known reciprocity theorem in classical optics [19].

Proceeding, we want to calculate the differential number of photons, emitted in the solid angle  $d\Omega$  and the spectral interval  $\omega, \omega + d\omega$ . For this we consider that a particle of a charge  $e_0$  with the law of motion  $\vec{r}(t)$  and the velocity  $\vec{v}(t) = d\vec{r}/dt$  generates a current, to be plugged in into Eq. (20). Then we take the asymptotic expression for the Green function Eq. (25) and substitute it into Eq. (24), which yields the electromagnetic field radiated in the far zone. This field is then used in the expression for the energy density

$$W_{\vec{n}\omega} = \frac{cr^2}{4\pi^2} |\vec{E}(\vec{r}, \omega)|^2. \quad (29)$$

Here  $\vec{n}$  is the unit vector directed towards the observation point  $\vec{n} = \vec{r}/r$ .

As a result the expression for the number of photons emitted in the solid angle  $d\Omega$  and the frequency range  $\omega, \omega + d\omega$  can be obtained [1]

$$\frac{\partial^2 N_{\vec{n}, \omega s}}{\partial \omega \partial \Omega} = \frac{e_0^2 \omega}{4\pi^2 \hbar c^3} \left| \int \vec{E}_{\vec{k}'s}^{(-)*}(\vec{r}(t), \omega) \vec{v}(t) e^{i\omega t} dt \right|^2, \quad (30)$$

where  $\vec{k}' = k\vec{n}$ .

With the help of the reciprocity theorem we can transform Eq. (30) into the form

$$\frac{\partial^2 N_{\vec{n}, \omega s}}{\partial \omega \partial \Omega} = \frac{e_0^2 \omega}{4\pi^2 \hbar c^3} \left| \int \vec{E}_{\vec{k}s}^{(+)}(\vec{r}(t), \omega) \vec{v}(t) e^{i\omega t} dt \right|^2, \quad (31)$$

$$\vec{k} = -\vec{k}',$$

where we have relabelled  $-\vec{k}'$  with  $\vec{k}$ .

Let us apply this approach and calculate the emitted number of quanta in the case of PXR-SPG. According to



Eq. (31) we first need to solve a diffraction problem and determine the electromagnetic field  $\vec{E}_{\vec{k}s}^{(+)}$ . For this we will apply the standard approach, namely the two-wave approximation of the dynamical diffraction theory [20, 21]. In this case two strong electromagnetic waves are excited in a crystal. The amplitudes of these waves satisfy a set of algebraic equations [1]

$$\begin{aligned} \left(\frac{k^2}{k_0^2} - 1 - \chi_0\right) E_{\vec{k}s} - c_s \chi_{-\vec{g}} E_{\vec{k}_g s} &= 0, \\ \left(\frac{k_g^2}{k_0^2} - 1 - \chi_0\right) E_{\vec{k}_g s} - c_s \chi_{\vec{g}} E_{\vec{k}s} &= 0. \end{aligned} \quad (32)$$

Here we introduced the scalar field amplitudes of the incident  $\vec{E}_{\vec{k}s}^{(+)} = \vec{e}_s E_{\vec{k}s}$  and diffracted  $\vec{E}_{\vec{k}_g s}^{(+)} = \vec{e}_{1s} E_{\vec{k}_g s}$  waves respectively. In addition,  $k_0 = \omega/c$ ,  $\vec{k}_g = \vec{k} + \vec{g}$ ,  $\vec{g}$  is the reciprocal lattice vector,  $\chi_0$  and  $\chi_{\vec{g}}$  are the Fourier components of the crystal susceptibility  $\chi(\vec{r})$

$$\chi(\vec{r}) = \sum_{\vec{g}} \chi_{\vec{g}} e^{i\vec{g} \cdot \vec{r}}. \quad (33)$$

The coefficient  $c_s = 1$  for the  $\sigma$  polarization ( $s = 1$ ) and  $c_s = \cos 2\theta_B$  for the  $\pi$  polarization ( $s = 2$ ) of the incident and diffracted waves respectively.

For the following we note that the waves of different polarizations propagate independently if we neglect terms of the order of  $\sim |\chi_0|^2$  in the Maxwell equations [20, 21].

The system of equations (32) is a system of homogeneous linear equations. Consequently, in order it to be solvable its determinant should vanish. This provides us the dispersion equation for  $k$  and determines the relations between amplitudes of incident and diffracted waves  $E_{\vec{k}s}$  and  $E_{\vec{k}_g s}$

$$\left(\frac{k^2}{k_0^2} - 1 - \chi_0\right) \left(\frac{k_g^2}{k_0^2} - 1 - \chi_0\right) - c_s^2 \chi_{\vec{g}} \chi_{-\vec{g}} = 0, \quad (34)$$

$$E_{\vec{k}_g s} = V_{\vec{k}s} E_{\vec{k}s}, \quad V_{\vec{k}s} = \frac{\left(\frac{k^2}{k_0^2} - 1 - \chi_0\right)}{c_s \chi_{-\vec{g}}}. \quad (35)$$

In Fig. 2 we show the propagation directions of electromagnetic waves in vacuum and in crystal respectively. We remind here that in the X-ray diffraction theory this type of geometry corresponds to the EAD case, namely grazing exit [20, 21]. As follows from Fig. 2 that in order to satisfy the boundary conditions on the interface one needs to take into account in vacuum not only an incident wave  $\vec{E}_{\vec{k}s}^{(0)}$ , but also a specularly reflected diffracted wave  $\vec{E}_{\vec{k}_g s}^{(sp)}$ , which defines the PXR-SPG

$$\vec{E}_{\vec{k}s}^{(0)} = \vec{e}_s e^{i\vec{k} \cdot \vec{r}}, \quad (36)$$

$$\vec{E}_{\vec{k}_g s}^{(sp)} = \vec{e}_{1s} E_{\vec{k}_g s}^{(sp)} e^{i(\vec{k}_{\parallel} + \vec{g}_{\parallel}) \cdot \vec{r}} e^{ik'_{gz} z}, \quad (37)$$

$$k'_{gz} = \sqrt{k_0^2 - (\vec{k}_{\parallel} + \vec{g}_{\parallel})^2}$$

The dispersion equation (34) is a fourth-order algebraic equation and consequently it has four solutions. For this reason there exist four electromagnetic waves in a crystal. However, two out of four these solutions are unphysical, since they lead to the exponentially growing field amplitudes inside the crystal. Consequently, when a boundary problem is solved only two waves should be taken into account. These waves have positive imaginary part of the  $k_z$ , i.e., the  $z$ -component of the wave vector inside a medium. According to the boundary conditions the in-plane components  $\vec{k}_{\parallel}$  of the wave vector are conserved. Therefore, the change of the wave vector is defined through the projection on the  $\vec{N}$  - the normal to the crystal surface [1]

$$\vec{k}_{s\mu} = \vec{k} - k_0 \epsilon_{\mu s} \vec{N}, \quad \mu = 1, 2, \quad (38)$$

where  $\vec{k} = k_0 \vec{n}$  and  $\vec{n}$  is the unit vector of the incident wave in vacuum. At the same time, the wave vector  $\vec{k}_g$  of the diffracted wave is directed parallel to the crystal surface and, therefore, the quantity  $|\nu_g| = |\vec{k}_g \cdot \vec{N}/k_0|$  is much smaller than unity, i.e.,  $|\nu_g| \ll 1$ . For the following we also define the quantity  $\nu_0 = \vec{k} \cdot \vec{N}/k_0$ .

We now plug in the expression (38) into the dispersion equation (32) and neglect the specularly reflected incident wave, which amplitude is proportional to  $|\chi_0|^2$  [20, 21] in the considered geometry. This yields the following cubic equation for the values of  $\epsilon_{s\mu}$

$$\begin{aligned} -2\nu_0 \epsilon_{\mu s}^3 + (4\nu_0 \nu_g - \chi_0) \epsilon_{\mu s}^2 + 2\nu_0 (\chi_0 - \alpha_B) \epsilon_{\mu s} \\ + \chi_0^2 - \chi_0 \alpha_B - c_s^2 \chi_{\vec{g}} \chi_{-\vec{g}} &= 0, \\ \alpha_B = \frac{k^2 - k_g^2}{k_0^2} = -\frac{2\vec{k} \cdot \vec{g} + g^2}{k_0^2}. \end{aligned} \quad (39)$$

In this equation the parameter  $\alpha_B$  defines the deviation from the Wulff-Bragg condition.

In the general case the solutions of this cubic equation are given through the cumbersome Cardano formula. However, these solutions can be significantly simplified if we employ the approximation, described in the Ref. [22]. For this we note that the angular spread of the PXR peak is given via a parameter  $\theta_0 \simeq \sqrt{|\chi_0|}$ . In addition, in the considered geometry  $|\nu_0| \approx 1$  and  $|\nu_g| \approx \sqrt{|\chi_0|} \gg |\chi_0|$ . In this approximation the desired solutions for the decaying fields inside a crystal are simplified and are equal to

$$\epsilon_{1s} = -\frac{\chi_0}{2\nu_0} + \frac{c_s^2 \chi_{\vec{g}} \chi_{-\vec{g}}}{2\nu_0 (\alpha_B + \chi_0)}, \quad (40)$$

$$\epsilon_{2s} = \nu_g + \sqrt{\nu_g^2 + \alpha_B + \chi_0}, \quad (41)$$

$$|\epsilon_{2s}| \sim \sqrt{|\chi_0|} \gg |\epsilon_{1s}| \sim |\chi_0|, \quad (42)$$

$$\epsilon_{2s}'' \sim \frac{\chi_0''}{\sqrt{|\chi_0|}} \gg \epsilon_{1s}'' \sim \chi_0''. \quad (43)$$

Having found solutions of the dispersion equation we can write down the solution of the Maxwell's equation in

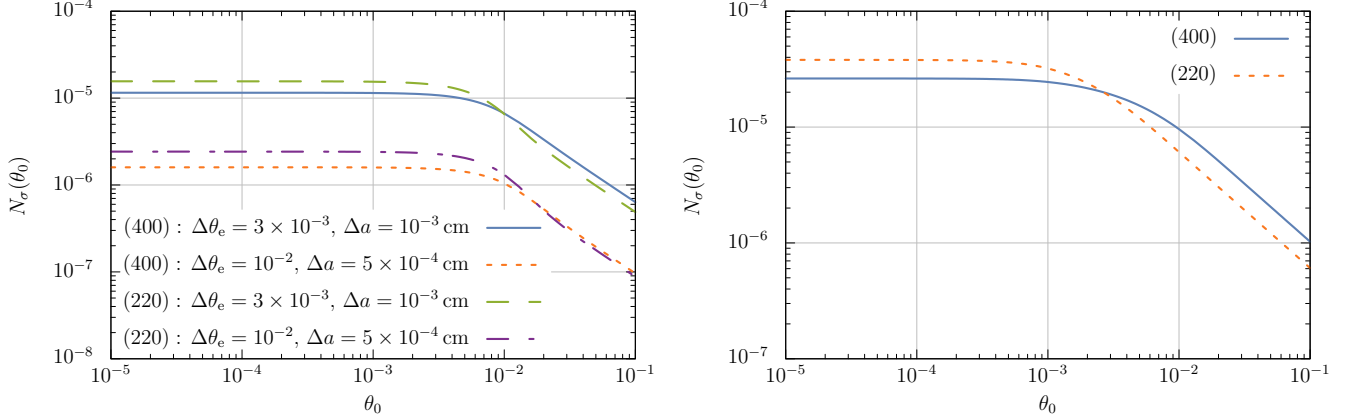


Figure 5: (Color online) Left pane: The dependence of the emitted number of quanta  $N_{\text{PXR-SPG}}$  on the incidence angle  $\theta_0$  for the MAMI facility. The electron energy  $E = 900$  MeV, the crystal length  $L = 1$  cm and the distance from the center of the beam to the crystal surface  $a_0 = 0.5 \times 10^{-3}$  cm. Right pane: The same dependence as on the left pane but for the LCLS facility. The electron energy  $E = 8000$  MeV, the crystal length  $L = 1$  cm, the electron beam spread  $\Delta a = 5 \times 10^{-3}$  cm and the distance from the center of the beam to the crystal surface  $a_0 = 2\Delta a$ .

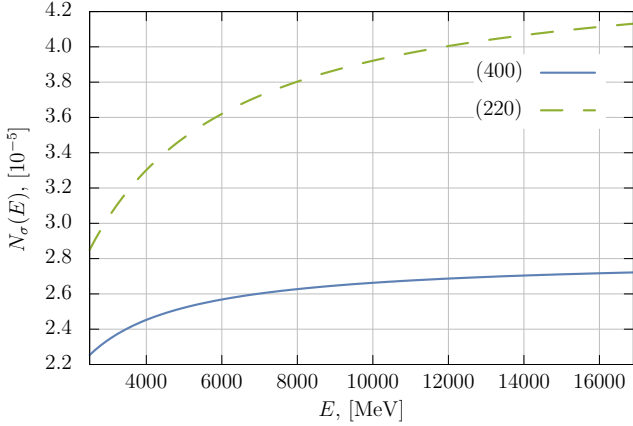


Figure 6: (Color online) The dependence of the total number of the emitted photons  $N_{\text{PXR-SPG}}$  on the electron beam energy for the LCLS facility. The parameters of the reflection are given via Eqs. (61), (62). The electron beam transverse size  $\Delta a = 5 \times 10^{-3}$  cm, the distance from the beam center to the crystal  $a_0 = 2\Delta a$ , the crystal length  $L = 1$  cm and the angle  $\theta_0 = 10^{-5}$  rad.

vacuum  $z > 0$  and inside a crystal  $z < 0$  as the following superposition

$$\vec{E}_{ks}^{(+)} = \vec{e}_s e^{i\vec{k} \cdot \vec{r}} + \vec{e}_{1s} E_s^{(sp)} e^{i(\vec{k}_{\parallel} + \vec{g}_{\parallel}) \cdot \vec{r}} e^{ik'_{gz} z}, \quad z > 0, \quad (44)$$

$$\vec{E}_{ks}^{(+)} = e^{i\vec{k} \cdot \vec{r}} \sum_{\mu=1,2} e^{-ik_0 z \epsilon_{\mu s}} (\vec{e}_s E_{\mu s} + \vec{e}_{1s} E_{g\mu s} e^{i\vec{g} \cdot \vec{r}}), \quad z < 0, \quad (45)$$

where the coordinate  $x$  is changing in the limits  $0 < x < L$ , with  $L$  being the crystal length (see Fig. 2).

In order to determine the amplitudes of these waves we require the continuity of the electromagnetic field on the crystal surface [20, 21], which in our case yields the system

of equations

$$\begin{aligned} E_{1s} + E_{2s} &= 1, \\ E_{g1s} + E_{g2s} &= E_s^{(sp)}, \\ (\nu_g - \epsilon_{1s})E_{g1s} + (\nu_g - \epsilon_{2s})E_{g2s} &= \nu'_g E_s^{(sp)}, \end{aligned} \quad (46)$$

where  $\nu'_g = k'_{gz}/k_0$ . The solution of this system of equations can be easily obtained, which reads

$$\begin{aligned} E_{1s} &= -\frac{(\chi_0 + 2\epsilon_{2s}\nu_0)(\nu'_g - \nu_g + \epsilon_{2s})}{(\epsilon_{1s} - \epsilon_{2s})[2\nu_0(\nu'_g - \nu_g + \epsilon_{2s} + \epsilon_{1s}) + \chi_0]}, \\ E_{2s} &= -\frac{(\chi_0 + 2\epsilon_{1s}\nu_0)(\nu'_g - \nu_g + \epsilon_{1s})}{(\epsilon_{1s} - \epsilon_{2s})[2\nu_0(\nu'_g - \nu_g + \epsilon_{2s} + \epsilon_{1s}) + \chi_0]}, \\ E_{g1s} &= -\frac{(\chi_0 + 2\epsilon_{1s}\nu_0)(\chi_0 + 2\epsilon_{2s}\nu_0)(\nu'_g - \nu_g + \epsilon_{2s})}{c_s \chi_{-g}(\epsilon_{1s} - \epsilon_{2s})[2\nu_0(\nu'_g - \nu_g + \epsilon_{2s} + \epsilon_{1s}) + \chi_0]}, \\ E_{g2s} &= -\frac{(\chi_0 + 2\epsilon_{1s}\nu_0)(\chi_0 + 2\epsilon_{2s}\nu_0)(\nu'_g - \nu_g + \epsilon_{1s})}{c_s \chi_{-g}(\epsilon_{1s} - \epsilon_{2s})[2\nu_0(\nu'_g - \nu_g + \epsilon_{2s} + \epsilon_{1s}) + \chi_0]}, \\ E_s^{(sp)} &= -\frac{(\chi_0 + 2\epsilon_{1s}\nu_0)(\chi_0 + 2\epsilon_{2s}\nu_0)}{c_s \chi_{-g}[2\nu_0(\nu'_g - \nu_g + \epsilon_{2s} + \epsilon_{1s}) + \chi_0]}. \end{aligned} \quad (47)$$

According to its definition, the PXR is emitted by a particles, which move uniformly. This corresponds to the following law of motion

$$\vec{r}(t) = \vec{r}_0 + \vec{v}t, \quad \vec{r}_0 = (0, 0, z_0), \quad (48)$$

where  $\vec{r}_0$  is the coordinate of an electron in the  $(x, z)$  plane, which is perpendicular to the crystal surface. In addition, we suppose that the  $r_{0y} = 0$  and in the moment of time  $t = 0$  the  $x$  coordinate of a particle is equal to zero, i.e.,  $x = 0$ .

When  $\vec{v} \perp \vec{N}$  the radiation is formed by the field of the diffracted wave, which propagates in the direction, defined via an electron velocity  $\vec{v}$  that is parallel to the vector  $\vec{k}_g = \vec{k} + \vec{g}$ , i.e.,  $\vec{v} \parallel \vec{k}_g$ . For this wave the Cherenkov condition

$\vec{v} \cdot \vec{k}_g = \omega/c$  can be fulfilled [16]. In our case the particle moves in vacuum, parallel to the crystal vacuum interface, which corresponds to  $z_0 < 0$ . Consequently, the radiation is defined by the specularly reflected diffracted wave  $E_s^{sp}$ .

Continuing, we plug in the law of motion (48) into Eq. (31) for the differential number of photons and integrate over the particle trajectory. This yields

$$\frac{\partial^2 N_{\vec{n}, \omega s}}{\partial \omega \partial \Omega} = \frac{e_0^2 \omega}{4\pi^2 \hbar c^5} (\vec{e}_{1s} \cdot \vec{v})^2 \times \left| E_s^{(sp)} L_g (1 - e^{-iL/L_g}) e^{ik'_{gz} z_0} \right|^2, \quad (49)$$

where

$$L_g = \frac{c}{\omega - v_x(k_x + g_x) - v_z k'_{gz}} \equiv \frac{1}{k_0 q},$$

$$q = 1 - \frac{v_x(k_x + g_x)}{\omega} - \frac{v_z k'_{gz}}{\omega}, \quad (50)$$

$$k'_{gz} = \sqrt{k_0^2 - (k_x + g_x)^2 - k_y^2}, \quad g_y = 0.$$

Here the quantity  $L_g$  determines the coherence length [23] for the radiation mechanism under investigation and  $k_0 q$  is the longitudinal component of the wave vector, which was transferred to the electron during the emission of a photon [16] ( $kq \approx (p_z - p_{1z})/\hbar - k_z$  with  $p_z$  and  $p_{1z}$  being the electron momenta before and after radiation of a photon correspondingly). The intensity of radiation has the maximal value for frequencies and angles of the emitted photons when the quantity  $|q^2|$  is minimal. In the considered geometry the following condition is fulfilled

$$v_x \approx v(1 - \theta_e^2/2) \gg v_z \approx v\theta_e, \quad (51)$$

where the angle  $\theta_e$  is the angle between the electron velocity and the crystal surface (see Fig. 2). Therefore, as follows from Eq. (50) the maximum of the coherence length is achieved when

$$q_0 = 1 - \frac{v_x(k_x + g_x)}{\omega} \approx 0,$$

$$\omega \approx \omega_B(1 - \theta_e^2/2 + \theta_x), \quad \omega_B = vg_x, \quad (52)$$

which defines the frequency of the PXR-SPG. Here  $\theta_x$  is the angle between the wave vector of the emitted photon and the normal  $\vec{N}$  to the crystal surface. We also note here that the frequency of the emitted radiation coincides with the frequency of the Smith-Purcell effect, when the period of the surface grating is equal to  $d = 2\pi/g_x$ .

In this frequency range the  $z$ -component of the wave vector  $k'_{gz}$  is purely imaginary, such that

$$k'_{gz} = \sqrt{k_0^2 - \frac{\omega^2}{v_x^2} - k_y^2} \approx ik_0 \sqrt{(\theta_x - \theta_{ez})^2 + \theta_y^2 + \theta_{ey}^2 + \gamma^{-2}} \equiv ik_0 \eta, \quad (53)$$

Consequently, the phase of the exponent  $\exp(ik'_{gz} z_0)$  in the Eq. (49) becomes real and the intensity of radiation exponentially decays with the increase of the distance from the crystal surface.

The field amplitude  $E_s^{(sp)}$  to be inserted in Eq. (49) significantly simplifies under the assumptions (42), (43) and looks like

$$E_s^{(sp)} = \frac{c_s \chi_g}{\alpha_B + \chi_0}. \quad (54)$$

In the Smith-Purcell geometry the angle  $\theta_B = \pi/4$ ,  $c_\sigma = 1$ ,  $c_\pi = \cos 2\theta_B \approx 0$ . This means that the emitted radiation will be polarized in the direction perpendicular to the plane defined by the vectors  $\vec{N}$  and  $\vec{g}$ . In addition, in the point where the intensity of radiation is maximal, which corresponds to  $q_0 = 0$ , the quantity  $\alpha_B$  exactly coincides with the one in the case of PXR-EAD [4]. That is

$$\alpha_B = -2[1 - v_0 \cos \theta \cos \theta_e - \theta_y \theta_{ey} - \theta_x \theta_{ez}] \approx -[\gamma^{-2} + (\theta_y - \theta_{ey})^2 + (\theta_x - \theta_{ez})^2]. \quad (55)$$

Combining together all expressions and plugging them into Eq. (49) we determine the spectral and angular distribution for the number of photons emitted per electron in the frequency range  $\omega, \omega + d\omega$ , in the solid angle  $d\Omega \approx d\theta_x d\theta_y$

$$\frac{\partial^3 N_\sigma}{\partial \omega \partial \theta_x \partial \theta_y} = \frac{e_0^2}{4\pi^2 \hbar \omega c} \frac{(\theta_y - \theta_{ey})^2 |\chi_g|^2}{[\gamma^{-2} + (\theta_y - \theta_{ey})^2 + (\theta_x - \theta_{ez})^2 - \chi_0']^2} \times \frac{[1 - 2 \cos(k_0 q_0 L) e^{-k_0 L \theta_{ez} \eta} + e^{-2k_0 L \theta_{ez} \eta}]}{q_0^2 + \theta_{ez}^2 \eta^2} \times e^{-2k_0 \eta |z_0|} \quad (56)$$

and all parameters of the medium are evaluated at the frequency  $\omega = \omega_B$ .

The integration with respect to frequency can be performed in the complex plane of the variable  $q_0$ , taking into account that  $dq_0 = d\omega/\omega_B$ . This yields

$$\frac{\partial^2 N_\sigma}{\partial \theta_x \partial \theta_y} = \frac{e_0^2}{4\pi \hbar c} \frac{(\theta_y - \theta_{ey})^2 |\chi_g|^2}{[\gamma^{-2} + (\theta_y - \theta_{ey})^2 + (\theta_x - \theta_{ez})^2 - \chi_0']^2} \times \frac{[1 - e^{-2k_0 L |\theta_{ez}| \eta}]}{|\theta_{ez}| \eta} e^{-2k_0 \eta |z_0|} \quad (57)$$

This equation defines the intensity of the emitted radiation from a part of the beam, which moves in vacuum  $z_0 > 0$ , parallel to the crystal vacuum interface, where the parameter  $\eta$  is defined as

$$\eta = \sqrt{(\theta_x - \theta_{ez})^2 + \theta_y^2 + \theta_{ey}^2 + \gamma^{-2}}. \quad (58)$$

According to Eq. (3) this electrons contribute to the Smith-Purcell intensity  $N_{SP}$ .

In contrast, electrons of a beam that are moving inside the crystal, i.e.,  $z_0 < 0$  emit radiation in the geometry



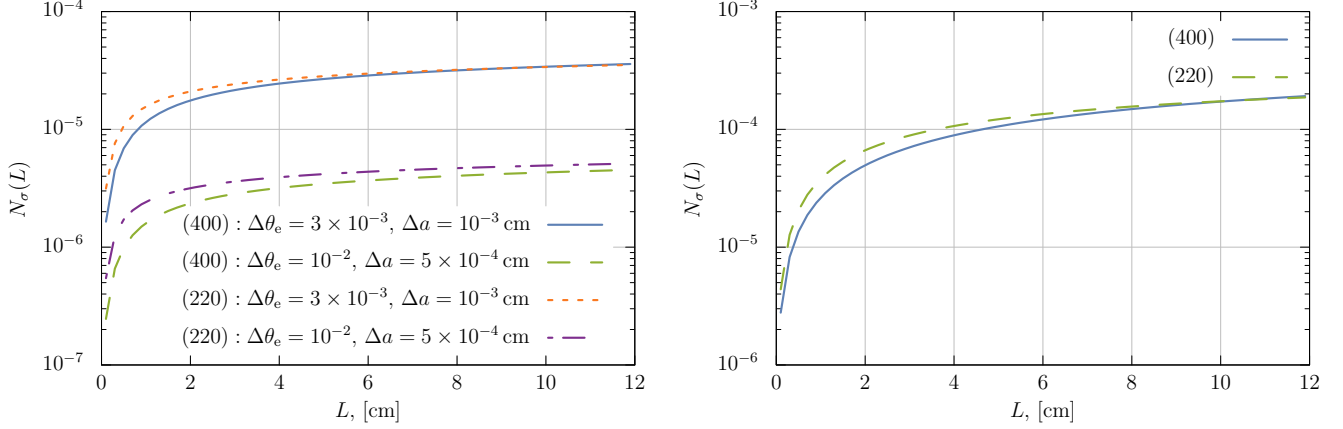


Figure 7: (Color online) Left pane: The dependence of the emitted number of quanta  $N_{\text{PXR-SPG}}$  on the crystal length  $L$  for the MAMI facility. The electron energy  $E = 900$  MeV, angle  $\theta_0 = 10^{-5}$  rad and the distance from the center of the beam to the crystal surface  $a_0 = 0.5 \times 10^{-3}$  cm. Right pane: The same dependence as on the left pane but for the LCLS facility. The electron energy  $E = 8000$  MeV, angle  $\theta_0 = 10^{-5}$  rad, the electron beam spread  $\Delta a = 5 \times 10^{-3}$  cm and the distance from the center of the beam to the crystal surface  $a_0 = 2\Delta a$ . In addition we assume that the electrons of a beam are described via distribution function (60) with the mean values of  $\theta_0$  and  $a_0$  respectively.

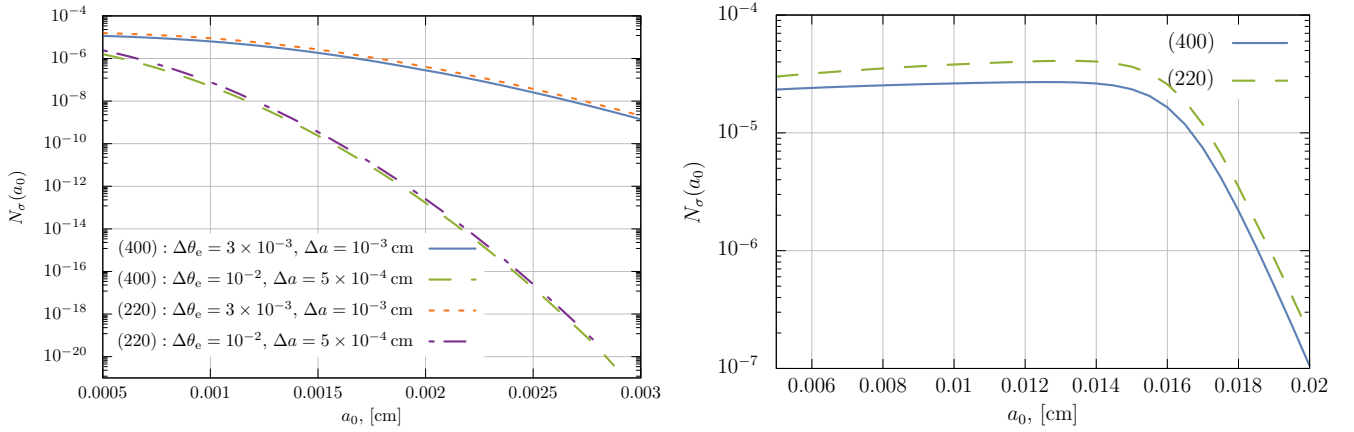


Figure 8: (Color online) Left pane: The dependence of the emitted number of quanta  $N_{\text{PXR-SPG}}$  on the distance from the beam center to the crystal surface  $a_0$  for the MAMI facility. The electron energy  $E = 900$  MeV, angle  $\theta_0 = 10^{-5}$  rad and the crystal length  $L = 1$  cm. Right pane: The same dependence as on the left pane but for the LCLS facility. The electron energy  $E = 8000$  MeV, angle  $\theta_0 = 10^{-5}$  rad, the electron beam spread  $\Delta a = 5 \times 10^{-3}$  cm and the crystal length  $L = 1$  cm.

of PXR-EAD, which was recently investigated in Ref. [4]. The differential number of photons emitted in this case reads

$$\frac{\partial^2 N_\sigma}{\partial \theta_x \partial \theta_y} = \frac{e_0^2}{4\pi\hbar c} \frac{(\theta_y - \theta_{ey})^2 |\chi_g|^2}{[\gamma^{-2} + (\theta_y - \theta_{ey})^2 + (\theta_x - \theta_{ez})^2 - \chi_0']^2} \times \frac{(1 - e^{-Lk_0\chi_0''|\theta_{ez}|})}{\chi_0''|\theta_{ez}|} e^{-\chi_0''k_0|z_0|}. \quad (59)$$

We notice here that the spectral angular distribution of the emitted photons depends on the parameters of the crystalline planes only through the components of dielectric susceptibilities.

In order to evaluate the total number of photons emitted by the bunch of electrons, one needs to integrate Eqs. (57), (59) over angles and average over the parameters of the electron beam. This is performed by making a convolution with the distribution functions over the initial posi-

tion  $z_0$  and the spreads of the electron angles  $\theta_{ey,z}$  due to the bunch emittance when  $z_0 > 0$  and, in addition, due to the multiple electron scattering when  $z_0 < 0$ . We consider the Gaussian distribution functions over the electron beam parameters that are given as

$$\begin{aligned} G(\theta_{ez}, \theta_{ey}, z_0) &= CF(\theta_{ez}, \theta_{ey}, z_0), \\ F &= \exp[-((\theta_{ez} - \theta_0)^2 + \theta_{ey}^2)/\Delta\theta_e^2] \\ &\quad \times \exp[-(z_0 - a_0)^2/\Delta a^2], \quad z_0 > 0 \\ F &= \exp[-(\theta_{ez}^2 + \theta_{ey}^2)/(\theta_s^2 + \Delta\theta_e^2)] \\ &\quad \times \exp[-(z_0 - a_0)^2/\Delta a^2], \quad z_0 < 0. \end{aligned} \quad (60)$$

Here the angle  $\theta_0$  is the incident angle of the electron beam and  $\Delta a$  and  $\Delta\theta_e$  are the transversal and angular spreads correspondingly. When the angle  $\theta_0$  is close to zero we have the grazing geometry of PXR-EAD and conversely, when it is large on has the conventional transition geome-

try of PXR. The constant  $C$  determines the normalization condition of the distribution. We choose it from requiring that the distribution is normalized to one

$$\int d\theta_{ez} d\theta_{ey} dz_0 G(\theta_{ez}, \theta_{ey}, z_0) = 1,$$

such that the total intensity is referred to the single electron, i.e., the total intensity from the electron bunch is divided by the number of electrons in the bunch.

Taking into account the above discussion, for the numerical evaluation we consider that the angle  $\theta_{ez}$  is counted from the angle  $\theta_0$  and introduce the polar coordinates  $\theta_x - \theta_0 = \rho \cos \varphi$ ,  $\theta_y = \rho \sin \varphi$ . The integration is then performed in the range  $\rho = [0, \theta_D]$  and  $\varphi = [0, 2\pi]$ , with  $\theta_D$  being the aperture of a detector. The result of this integration is then convoluted with the distribution function given via Eq. (60).

#### 4. Numerical results and discussion

In this section we present numerical results of the calculation of the total number of photons  $N_{\text{PXR-SPG}}$  emitted by a single electron in the Smith-Purcell geometry. We choose the most intense PXR peaks for the (400) and (220) reflections in the Si crystal [24]. For these reflections the following parameters, taken from the X-ray database [25] are employed. For the reflection (400)

$$\begin{aligned} \hbar\omega_B &= 6.45 \text{ keV}, & k_0 &= 3.29 \times 10^8 \text{ cm}^{-1}, \\ \chi'_0 &= -0.24 \times 10^{-4}, & \chi''_0 &= 0.83 \times 10^{-6}, \\ \chi'_g &= 0.12 \times 10^{-4}, & \chi''_g &= 0.71 \times 10^{-6} \end{aligned} \quad (61)$$

and (220)

$$\begin{aligned} \hbar\omega_B &= 4.51 \text{ keV}, & k_0 &= 2.3 \times 10^8 \text{ cm}^{-1}, \\ \chi'_0 &= -0.48 \times 10^{-4}, & \chi''_0 &= 0.32 \times 10^{-5}, \\ \chi'_g &= 0.29 \times 10^{-4}, & \chi''_g &= 0.31 \times 10^{-5}. \end{aligned} \quad (62)$$

respectively. In addition we consider that the aperture of the detector  $\theta_D = 10^{-2}$ .

As a typical scenario we have investigated two accelerator facilities, namely Mainz microtron MAMI [13, 14, 26], where the typical electron beam energy  $\approx 900 \text{ MeV}$  and SLAC Linac Coherent Light Source LCLS [27–29], where the electron beam energy varies from  $2500 \text{ MeV}$  to  $16900 \text{ MeV}$ . The MAMI facility provides the electron beam with natural emittance  $\epsilon = 5 \times 10^{-6} \text{ cm} \times \text{rad}$ , while the normalized emittance on the LCLS facility  $\gamma\epsilon = (0.5 - 1.6) \times 10^{-4} \text{ cm} \times \text{rad}$ . For the MAMI accelerator we assume that two different electron beams with similar emittances, but different transverse sizes and angular spreads are employed in the experiment, viz.  $\epsilon = 5 \times 10^{-6} \text{ cm} \times \text{rad}$  with  $\Delta\theta_e = 10^{-2} \text{ rad}$ ,  $\Delta a = 5 \times 10^{-4} \text{ cm}$  and  $\epsilon = 3 \times 10^{-6} \text{ cm} \times \text{rad}$ , with  $\Delta\theta_e = 3 \times 10^{-3} \text{ rad}$ ,  $\Delta a = 10^{-3} \text{ cm}$ .

In all following figures we plot the emitted number of quanta normalized by the number of electrons, i.e., the total intensity is divided by the number of electrons.

##### 4.1. The ideal case of a vanishing emittance

We start a discussion from an ideal case when an electron beam does not possess an emittance. In this situation the integration with a distribution function  $G(\theta_{ez}, \theta_{ey}, z_0)$  can be performed analytically. For this we note that when  $\Delta a \rightarrow 0$  and  $\Delta\theta_e \rightarrow 0$  the distribution is localized near point  $z_0 = a_0$ . We now fix the value  $a_0 > 0$ . In this situation the only contribution to the integral is coming from the region  $[0, \infty)$ . Consequently, we continue the integration to the region  $(-\infty, \infty)$  and integrate the differential number of quanta (57) with the distribution  $\delta(z_0 - a_0)\delta(\theta_{ez})\delta(\theta_{ey})$ . Performing this we are left with an integral over  $pd\rho d\varphi$ . The integral in  $\varphi$  is trivially performed and we arrive to

$$N_{\text{SP}}^{\text{ideal}} = \frac{k_0 L}{2} \frac{e_0^2}{\hbar c} |\chi_g|^2 \times \int_{\gamma^{-1}}^{\sqrt{\theta_D^2 + \gamma^{-2}}} dt \frac{t(t^2 - \gamma^{-2})}{(t^2 - \chi'_0)^2} e^{-2k_0 a_0 t}. \quad (63)$$

This integral can be computed analytically and expressed through the exponential integral function  $\text{Ei}(x)$ . However, the resulting expression is rather cumbersome and we do not list it here.

The dependence on the main parameters can be deduced from Eq. (63). Thus, the emitted number of quanta is proportional to the crystal length and exponentially decays with the increasing value of the impact parameter  $a_0$ . For ultra-relativistic electrons the dependence on the energy is weak and is given via  $\text{const} + O(\gamma^{-2})$ . Concluding, in Fig. 3 we plot the dependence of the total emitted number of quanta  $N_{\text{SP}}^{\text{ideal}}$  on the impact parameter  $a_0$ . As can be seen from the figure  $N_{\text{SP}}^{\text{ideal}}$  quickly decays and for realistic impact parameters is negligible.

At the same time, when the impact parameter  $a_0 = 0$  the intensity of SP can be comparable with the intensity of PXR-EAD [4], since both are  $\sim 10^{-5}$  (see Fig. 3 and Ref. [4]).

##### 4.2. The realistic situation of non-vanishing emittance

We now introduce the restrictions coming from the realistic emittances of experimental facilities. First of all, we compare the relative contributions into the total radiation intensity  $N_{\text{PXR-SPG}}$  from the parts of the electron beam that are moving in crystal and in vacuum (pure SP radiation) respectively, analogously to the ideal case. According to the qualitative estimation (14) and Eq. (63) of the ideal case the Smith-Purcell radiation can be significant when the beam propagates close to the crystal surface ( $a_0$  is small) and possesses a small transversal width  $\Delta a$ . Consequently, in Fig. 4 we plot the dependence of  $N_{\text{SP}}$  on  $a_0$ , when  $\Delta a = a_0/2$ . As follows from the figure, for a realistic beam size the relative contribution of this part is small, which agrees with the qualitative estimation of Eq. (14) and with the ideal case investigated above.

Proceeding we would like to verify that since the value of  $N_{\text{SP}}$  is small the main contribution to  $N_{\text{PXR-SPG}}$  is

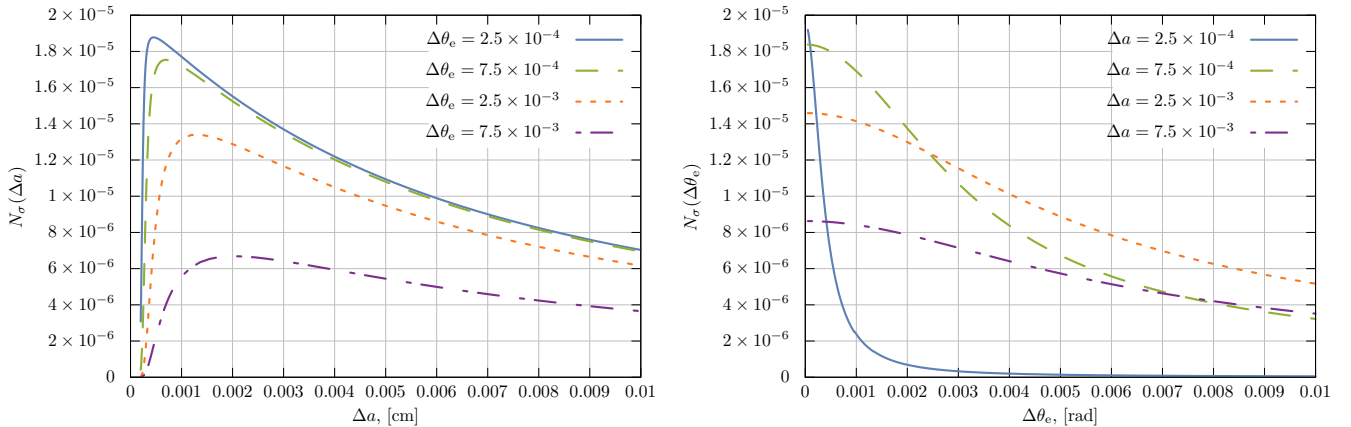


Figure 9: (Color online) Left pane: The dependence of the emitted number of quanta on the beam transversal size  $\Delta a$  for the MAMI facility. The electron energy  $E = 900$  MeV, angle  $\theta_0 = 10^{-5}$  rad, the distance to the crystal  $a_0 = 0.5 \times 10^{-3}$  cm and the crystal length  $L = 1$  cm. Right pane: The dependence of the emitted number of quanta on the beam angular spread  $\Delta \theta_e$  for the MAMI facility. The parameters of the electron beam are the same as on the left pane.

coming from the tail of the electron beam (beam halo), which is moving inside a crystal and, consequently, is given via PXR-EAD. For this we plot in Fig. 5 the results of the numerical evaluation of the total number of photons  $N_{\text{PXR-SPG}}$  emitted by a beam of electrons normalized by the number of electrons as a function of the beam entrance angle  $\theta_0$ . In addition we consider that the crystal length  $L \gg L_{\text{abs}} = (k_0 \chi_0'')^{-1}$ , which is a realistic scenario. In this situation we expect to observe a similar dependence as in our previous work [4]. As follows from Fig. 5 the number of photons is significantly increasing when the angle  $\theta_0 < [L k_0 \chi_0'']^{-1} = L_{\text{abs}}/L$ , which renders our hypothesis as the correct one.

As a result the dependence of  $N_{\text{PXR-SPG}}$  on various parameters of the beam are analogous to the ones, which were investigated in the Ref [4]. In particular, in Fig. 6 we plot the dependence of  $N_{\text{PXR-SPG}}$  on the beam energy, when the crystal length  $L$  is fixed. The dependence  $N_{\text{PXR-SPG}}(E)$  after reaching some  $E_{\text{opt}}$  saturates. The value  $E_{\text{opt}}$  is determined by the parameters of the crystal.

In Fig. 7 we plot the dependence of the number of emitted quanta on the crystal length  $L$ , when the electron energy is fixed at  $E = 900$  MeV at MAMI and at  $E = 8000$  MeV at LCLS. When the crystal length increases to  $L_{\text{opt}} \approx 2$  cm the PXR intensity saturates. For crystal lengths  $L > L_{\text{opt}}$  the intensity slowly grows.

A specific peculiarity of PXR-SPG is a strong dependence of the radiation intensity on the distance  $a_0$  to the crystal surface. Therefore, in Fig. 8 we plot the dependence on  $a_0$ . As follows from the figure, when the parameter  $a_0$  increases the intensity exponentially decreases.

With this we can conclude that practically under realistic experimental conditions it is impossible to observe pure SP radiation, since it is few order of magnitude less than the corresponding PXR-EAD. Nevertheless, the geometry of PXR-SPG can be exploited for the non-destructive diagnosis of the electron beam, due to its strong dependence

on an electron emittance that can be used as a complement to the conventional knife-edge method [30, 31]. For this reason, in Fig. 9 we show the dependence of the radiation intensity on the parameters of the electron beam  $\Delta a$  and  $\Delta \theta_e$ . It can be concluded that both components of the emittance influence the radiation intensity, which can be useful for the diagnosis of relativistic electron beams. It is essential that the radiation is formed only by a small part of the beam corresponding to the tail of its angular distribution and consequently the characteristics of the majority of the electrons are not changed.

## 5. Conclusions

In our work we have investigated the PXR radiation in the Smith-Purcell geometry (PXR-SPG), when an electron beam propagates in *vacuum* parallel to the crystal-vacuum interface. We have developed a theory, which describes this phenomenon and is based on the dynamical diffraction theory. Our approach takes into account peculiar features due to the grazing incidence of an electron beam on a crystal surface. The reciprocity theorem allowed us to express the spectral-angular distribution of the radiation intensity only through the solutions of the homogeneous Maxwell equations.

We have demonstrated that the total number of photons  $N_{\text{PXR-SPG}}$ , emitted in the PXR peak is mainly given by the electrons which are moving inside a crystal, while the pure SP radiation is few order of magnitudes smaller than its PXR-EAD counterpart.

At the same time, since the PXR-SPG radiation is mainly formed by the beam halo, which moves inside a crystal and the total number of emitted photons strongly depends on the parameters of an electron beam, that is on both components of an electron emittance  $\Delta a$  and  $\Delta \theta_e$ , it can be used for non-destructive diagnosis tool for relativistic electron beams.

## 6. Acknowledgements

ODS is grateful to C. H. Keitel for helpful discussions.

## Appendix A. List of notations for electromagnetic waves

- $\vec{E}_{ks}^{(\pm)}(\vec{r}, \omega)$  — Solutions of the homogeneous Maxwell equations for the ingoing – (outgoing +) electromagnetic waves.
- $E_{ks}$  and  $E_{kgs}$  — Magnitudes of the direct and diffracted waves in a crystal respectively.
- $\vec{E}_{ks}^{(0)}$  — Incident (direct) electromagnetic wave.  $E_{ks}^{(0)}$  its magnitude.
- $\vec{E}_{kgs}^{(sp)}$  — Specular reflected diffracted wave in vacuum.  $E_{kgs}^{(sp)}$  its magnitude.
- $E_{\mu s}$  and  $E_{g\mu s}$  ( $\mu = 1, 2$ ) — Magnitudes of the direct and diffracted waves inside a crystal, which correspond to the different solutions of the dispersion relation.

In addition, the diffraction of the wave with the vector  $\vec{k}'$  in Fig. 1 happens on the crystallographic planes described by the reciprocal vector  $\vec{g}'$ . At the same time, the diffraction of the wave with the vector  $\vec{k} = -\vec{k}'$  is happening on the planes with the reciprocal vector  $\vec{g}$  (see Fig. 2).

## References

- [1] V. G. Baryshevsky, I. D. Feranchuk, and A. P. Ulyanenko, *Parametric X-Ray Radiation in Crystals: Theory, Experiment and Applications (Springer Tracts in Modern Physics)* (Springer, 2006).
- [2] Feranchuk, I.D. and Ivashin, A.V., *J. Phys. France* **46**, 1981 (1985).
- [3] J. Hyun, M. Satoh, M. Yoshida, T. Sakai, Y. Hayakawa, T. Tanaka, K. Hayakawa, I. Sato, and K. Endo, *Phys. Rev. Accel. Beams* **21**, 014701 (2018).
- [4] O. Skoromnik, V. Baryshevsky, A. Ulyanenko, and I. Feranchuk, *Nuclear Instruments and Methods in Physics Research Section B: Beam Interactions with Materials and Atoms* **412**, 86 (2017).
- [5] S. J. Smith and E. M. Purcell, *Phys. Rev.* **92**, 1069 (1953).
- [6] P. M. van den Berg, *J. Opt. Soc. Am.* **63**, 689 (1973).
- [7] H. L. Andrews and C. A. Brau, *Phys. Rev. ST Accel. Beams* **7**, 070701 (2004).
- [8] V. Baryshevsky and A. Gurinovich, *Nuclear Instruments and Methods in Physics Research Section B: Beam Interactions with Materials and Atoms* **252**, 92 (2006).
- [9] M. J. Moran, *Phys. Rev. Lett.* **69**, 2523 (1992).
- [10] D. Y. Sergeeva, A. A. Tishchenko, and M. N. Strikhanov, *Phys. Rev. ST Accel. Beams* **18**, 052801 (2015).
- [11] M. Kumar, L. K. Babbar, R. K. Deo, T. A. Puntambekar, and V. K. Senecha, *Phys. Rev. Accel. Beams* **21**, 052801 (2018).
- [12] V. Ginzburg, *Theoretical Physics and Astrophysics*, International Series on Nuclear Energy (Elsevier Science, 2013).
- [13] K. H. Brenzinger, C. Herberg, B. Limburg, H. Backe, S. Dambach, H. Euteneuer, F. Hagenbuck, H. Hartmann, K. Johann, K. H. Kaiser, O. Kettig, G. Knies, G. Kube, W. Lauth, H. Schöpe, and T. Walcher, *Zeitschrift für Physik A Hadrons and Nuclei* **358**, 107 (1997).
- [14] W. Lauth, H. Backe, O. Kettig, P. Kunz, A. Sharafutdinov, and T. Weber, *The European Physical Journal A - Hadrons and Nuclei* **28**, 185 (2006).
- [15] V. Baryshevsky, I. Feranchuk, A. Grubich, and A. Ivashin, *Nuclear Instruments and Methods in Physics Research Section A: Accelerators, Spectrometers, Detectors and Associated Equipment* **249**, 306 (1986).
- [16] Baryshevsky, V.G. and Feranchuk, I.D., *J. Phys. France* **44**, 913 (1983).
- [17] H. Nitta, *Journal of the Physical Society of Japan* **69**, 3462 (2000).
- [18] V. Baryshevsky, *High-energy Nuclear Optics of Polarized Particles* (World Scientific, 2012).
- [19] M. Born and E. Wolf, *Principles of Optics: Electromagnetic Theory of Propagation, Interference and Diffraction of Light* (Elsevier Science, 2013).
- [20] A. Authier, *Dynamical Theory of X-ray Diffraction*, International Union of Crystallography monographs on crystallography (Oxford University Press, 2001).
- [21] A. Benediktovich, I. Feranchuk, and A. Ulyanenko, *Theoretical Concepts of X-Ray Nanoscale Analysis: Theory and Applications*, Springer Series in Materials Science (Springer Berlin Heidelberg, 2013).
- [22] V. M. Kaganer, V. L. Indenbom, M. Vrána, and B. Chalupa, *Physica Status Solidi (a)* **71**, 371 (1982).
- [23] V. M. Galitsky and I. I. Gurevich, *Il Nuovo Cimento (1955-1965)* **32**, 396 (1964).
- [24] B. Sones, Y. Danon, and R. Block, *Nuclear Instruments and Methods in Physics Research Section B: Beam Interactions with Materials and Atoms* **227**, 22 (2005), radiation from Relativistic Electrons in Periodic Structures (RREPS'03).
- [25] S. A. Stepanov, "X-ray dynamical diffraction web server," <http://x-server.gmca.aps.anl.gov/>, accessed: 14-07-2018.
- [26] K.-H. Brenzinger, B. Limburg, H. Backe, S. Dambach, H. Euteneuer, F. Hagenbuck, C. Herberg, K. H. Kaiser, O. Kettig, G. Kube, W. Lauth, H. Schöpe, and T. Walcher, *Phys. Rev. Lett.* **79**, 2462 (1997).
- [27] LCLS authors, "LCLS Parameters – Update December 2017," [https://portal.slac.stanford.edu/sites/lclscore\\_public/Accelerator\\_Physics\\_Published\\_Documents/LCLS-parameters-3-22-17.pdf](https://portal.slac.stanford.edu/sites/lclscore_public/Accelerator_Physics_Published_Documents/LCLS-parameters-3-22-17.pdf), accessed: 12-12-2018.
- [28] Y. Ding, A. Brachmann, F.-J. Decker, D. Dowell, P. Emma, J. Frisch, S. Gilevich, G. Hays, P. Hering, Z. Huang, R. Iverson, H. Loos, A. Miahnahri, H.-D. Nuhn, D. Ratner, J. Turner, J. Welch, W. White, and J. Wu, *Phys. Rev. Lett.* **102**, 254801 (2009).
- [29] R. Akre, D. Dowell, P. Emma, J. Frisch, S. Gilevich, G. Hays, P. Hering, R. Iverson, C. Limborg-Deprey, H. Loos, A. Miahnahri, J. Schmerge, J. Turner, J. Welch, W. White, and J. Wu, *Phys. Rev. ST Accel. Beams* **11**, 030703 (2008).
- [30] N. Smolyakov, H. Yoshida, and A. Hiraya, *Nuclear Instruments and Methods in Physics Research Section A: Accelerators, Spectrometers, Detectors and Associated Equipment* **448**, 73 (2000).
- [31] J. Bok, V. Kolařík, M. Horáček, M. Matějka, and F. Matějka, *Journal of Vacuum Science & Technology B* **31**, 031603 (2013), <https://doi.org/10.1116/1.4802920>.